ELSEVIER

Contents lists available at ScienceDirect

Journal of Non-Crystalline Solids

journal homepage: www.elsevier.com/locate/jnoncrysol





Formation and properties of biocompatible Ti-based bulk metallic glasses in the Ti-Cu-Zr-Fe-Sn-Si-Ag system

Wei Yang ^a, Ying Liu ^b, Nengbin Hua ^c, Shujie Pang ^{a,d,*}, Yan Li ^{a,d}, Peter K. Liaw ^e, Tao Zhang ^{a,*}

- ^a Key Laboratory of Aerospace Materials and Performance (Ministry of Education), School of Materials Science and Engineering, Beihang University, Beijing, 100191, China
- ^b AVIC Manufacturing Technology Institute, Beijing, 100024, China
- ^c Department of Materials Science and Engineering, Fujian University of Technology, Fuzhou, 350118, China
- ^d Advanced Innovation Center for Biomedical Engineering, Beihang University, Beijing, 100191, China
- e Department of Materials Science and Engineering, The University of Tennessee, Knoxville, TN 37996, USA

ARTICLE INFO

Keywords: Biomaterial Metallic glass Titanium alloy Corrosion Biocompatibility

ABSTRACT

The Ni-free Ti-based bulk metallic glasses (BMGs) with high glass-forming ability (GFA) can be synthesized in the (Ti, Cu, Zr) $_{92.5}$ Fe $_{2.5}$ Sn $_2$ Si $_1$ Ag $_2$ alloy system over a wide composition range by copper-mold casting. Especially, the Ti $_{48}$ Cu $_{37}$ Zr $_{7.5}$ Fe $_{2.5}$ Sn $_2$ Si $_1$ Ag $_2$ glassy alloy can form the BMG rod with a diameter up to 6 mm and showed a high compressive strength of ~ 2.05 GPa, elastic modulus of ~ 100 GPa, and microhardness of ~ 571 Hv. The Ti-based BMGs presented good bio-corrosion resistance in a simulated physiological environment attributed to the formation of Ti-, Zr-, Si-, and Fe-enriched passive films. The biocompatibility of the Ti-based glassy alloys was systematically investigated by both indirect cytotoxicity test and direct cell-culture experiments. The Ti-based BMG extracts had no cytotoxic effects on the proliferation of the cells. The good cell adhesion, proliferation, differentiation, and mineralization of bone-forming MC3T3-E1 pre-osteoblasts on the BMGs were parallel to those on the Ti-6Al-4V alloy. These results manifested that the present Ti-based BMGs are promising candidates as biomaterials.

1. Introduction

Metallic biomaterials are widely used in implant devices, especially reconstruction of a failed hard tissue, including dental implants, permanent implants (e.g., joint implants), and temporary devices (e.g., bone screws and pins) due to their good mechanical properties, flexible workability and durability [1–4]. Compared with other commonly-used metallic biomaterials (e.g., the Co-Cr-based alloys and stainless steels), the Ti alloys with the combination of relatively-low elastic moduli and great corrosion resistance and biocompatibility have garnered great attention as biomedical materials [5–8]. However, for the long-term implantations, some problems of Ti alloys need to be overcome, such as the relatively low wear resistance related to particle disease, the host tissue damage and the immune rejection, etc. [2,3,5]. Therefore, exploring novel biomedical alloys with suitable mechano- and bio-compatibility is of great significance.

Bulk metallic glasses (BMGs) with a unique amorphous structure free from defects, like dislocations and crystalline boundaries, exhibit

Received 13 April 2021; Received in revised form 9 June 2021; Accepted 9 July 2021

superior mechanical properties and high corrosion resistance [9,10]. They also possess good net-shaping and thermoplastic-forming ability in the supercooled liquid region, which are beneficial for fabricating the implants in complex geometries with high dimensional accuracy [9,11]. Because of these comprehensive properties, great efforts have been devoted to developing novel BMGs for the biomedical purpose and evaluating their feasibility as biomaterials by in vitro and in vivo testing [10,12-15]. Among the BMG systems, Ti-based BMGs have attracted attention due to their good biocompatibility and the distinctive osseointegration of titanium [1,5,12]. As is well known, most Ti-based metallic glasses with high glass-forming ability (GFA) usually contain highly-toxic elements Be and Ni that would cause the long-term biosafety issues [16-20]. In the last decades, some Be- and Ni-free Ti-based metallic glasses have been developed in the Ti-Zr-Fe-Si [21], [22], [23], Ti-Zr-Nb-Si Ti–Zr–Ta–Si Ti-Cu-Hf-Si Ti-Zr-Cu-Fe-Sn-Si [25], and Ti-Zr-Nb-Hf-Si [26] systems. These Ti-based metallic glasses present good mechanical properties and corrosion resistance in various physiological solutions, such as the

E-mail addresses: pangshujie@buaa.edu.cn, pangshujie@hotmail.com (S. Pang), zhangtao@buaa.edu.cn (T. Zhang).

^{*} Corresponding author.

Hank's solution [21], Ringer's solution [22], and phosphate-buffered saline (PBS) [25], etc. However, their rather low GFA limits the applications in biomedical fields. The Ti–Zr–Cu–Pd(–Sn) BMGs present superior GFA, whereas the high content of the noble metal Pd is disadvantageous for the cost of their productions [27,28].

In our previous study, it has been found that the Ti₄₇Cu₃₈Zr_{7.5-} Fe_{2.5}Sn₂Si₁Ag₂ alloy free from Ni and Be possesses high GFA and can be prepared into bulk glassy rods with a diameter up to 7 mm [29]. Moreover, the Ti-based BMG presents superior mechanical properties and anti-corrosion performance, and can support the initial cell attachment and proliferation [29,30]. Therefore, in this study, the metallic glasses in the Ti-Zr-Cu-Fe-Sn-Si-Ag system were systemically investigated to find new Ti-based BMGs with high GFA, which are suitable for biomedical applications. The composition range for forming BMGs in the (Ti, Cu, Zr)_{92.5}Fe_{2.5}Sn₂Si₁Ag₂ (atomic percent, at%) alloys, the mechanical properties and corrosion behaviors were examined. The present work further studied the biocompatibility of the present BMGs in detail. Both indirect cytotoxicity test and direct cell-culture experiments, including cell adhesion, proliferation, differentiation and mineralization, were carried out, using the bone-forming MC3T3-E1 pre-osteoblasts. The related mechanisms are also discussed.

2. Materials and methods

2.1. Materials preparation

Alloy ingots of Ti_{92.5-x-v}Cu_xZr_vMAg₂ and Ti₄₇Cu₄₀Zr_{7.5}M (at.%), where M represents the combination of Fe2.5Sn2Si1 for convenience, were fabricated by arc-melting the mixtures of the pure metals in a Tigettered argon atmosphere. The ribbon specimens of about 30 µm in thickness and 2 mm in width were fabricated by melt-spinning, and the rod specimens with diameters of 2 – 5 mm and a length of 50 mm and the plate samples ($50 \times 10 \times 1 \text{ mm}^3$) were obtained by injection casting. The larger specimens were fabricated by tilt-pouring casting. For mechanical testing, the specimens (ϕ 2 mm \times 4 mm) were cut from the rods with a low-speed diamond saw. For bio-corrosion and biocompatibility tests, the glassy specimens (ϕ 6 mm \times 1 mm) were machined from the plate samples by electro-discharge machining, and commercial Ti-6Al-4V alloy (denoted as Ti64) specimens with the same geometry were used as the reference material. Surfaces of these specimens were prepared in the same procedure as that presented in Ref. [29]. For the biocompatibility tests, the specimens were sterilized by the 1-hour ultraviolet (UV) light.

2.2. Microstructure and mechanical tests

Microstructure of the cast specimens with different diameters was examined by a Bruker AXS D8 X-ray diffraction (XRD, Cu-K\$\alpha\$). Transmission electron microscopy (TEM) observation was carried out with a JEM 2100F TEM. Thermal behaviors were analyzed at a heating rate of 0.33 K/s by the NETZSCH 404C differential scanning calorimetry (DSC). Compressive mechanical properties were conducted at a strain rate (2.0 $\times~10^{-4}~s^{-1}$) with a SANS CMT5504 testing machine. After the deformation, the samples were observed, using a JEOL JSM-6010LA scanning electron microscope (SEM). Vickers microhardness was performed with a Vickers microhardness tester (Future-tech FM800) at a 200-gf load for 15 s. An ultrasound velocity measurement (Olympus Panametrics-NDT 5703PR) was employed to characterize the Young's modulus (E). The densities of the BMGs were determined according to the Archimedean principle, using the deionized water.

2.3. Bio-corrosion resistance characterization

The immersion and electrochemical tests in the PBS at 310 K were performed to examine the bio-corrosion behaviors of the BMGs [31]. The electrochemical tests were examined, employing a Princeton

VersaSTAT III electrochemical workstation and a three-electrode system consisting of a sample as the working electrode, a saturated calomel reference electrode (SCE) and a platinum counter electrode. After the samples were kept in the PBS for 1,800 s to achieve a steady open-circuit potential (OCP), anodic polarization tests were started from the potential of 0.5 V below the OCPs. For the immersion experiments, specimens were immersed in the PBS referring to ASTM-G31-72 standard [32]. After 30-day immersion in the PBS, a weight loss of the studied Ti alloys was measured, using an analytical balance with a precision of 1×10^5 g, and the corrosion rates were determined by the weight loss. An ESCA-LAB250 X-ray photoelectron spectroscopy (XPS, Al-Kα) was employed to study the passive films formed on the BMGs after the immersion for 30 days. The XPS spectra were further analyzed, using the XPSPEAK 4.1 analytical software. An Agilent 7800 inductively-coupled plasma-mass spectrometry (ICP-MS) was employed to monitor the ion concentrations dissolved into the PBS.

2.4. Cellular behaviors

Mouse MC3T3-E1 pre-osteoblasts were cultured in a minimum essential medium (MEM) supplemented with 10 % fetal bovine serum (FBS) in the incubator (310 K, 5 vol.% $\rm CO_2$). The medium was changed every 3 days. Cells were harvested with 0.25% trypsin and ethylenediaminetetraacetic acid (EDTA) and used for cellular-behavior investigation.

2.4.1. Cell adhesion and morphology

Cells were seeded on the surface of each alloy at a density of 5×10^3 cells/well. After 4-hour incubation, the specimens were fetched out and immersed with the PBS. Then the cells were fixed and dehydrated according to the procedure described in Ref. [33]. The morphologies of the adhered cells were observed, using SEM. For the adhered cell number quantification, images of five randomly-selected areas on the surfaces of each alloy were utilized by the ImageJ software (NIH, USA).

2.4.2. Cytoskeleton organization

Fluorescent staining of actin filaments demonstrates the development of actin cytoskeleton. After the incubation for 4 h, the cells were fixed with 4% paraformaldehyde (Beyotime Biotech) and permeabilized with 0.1% Triton X-100 (Beyotime Biotech) in the PBS, for 15 min. each. To label the actin filaments, samples were incubated with a fluorescein isothiocyanate (FITC)-phalloidin (Actin-tracker green, Beyotime Biotech) for 1 h, followed by rinsing with PBS. Subsequently, cell nuclei were stained with 4',6-diamindino-2-phenylindole (DAPI, Beyotime Biotech) for 5 min.. After rinsing with PBS, the specimens were mounted on a coverslip with an antifade-mounting medium (Beyotime Biotech). Then, the fluorescent images were viewed under fluorescence microscopy (Olympus IX71).

2.4.3. Cell proliferation and cytotoxicity evolution

The cell-proliferation behavior was measured by a water-soluble tetrazolium salt (WST-1 assay) at time points of 2, 4, and 7 days. At each harvest time, $10~\mu$ l WST-1 was added to each well, and samples were further cultured with WST-1 for 4 h. The optical density (O.D.) was recorded at 450 nm on a plate reader (BioTek) against a blank control.

Cytotoxicity tests of the BMGs were examined by the indirect contact based on the procedure ISO 10993-5:2009 [34], using the sample extracts and the WST-1 assay. The sample extracts were prepared by immersing the alloys in MEM with a ratio of the surface area to the extraction medium volume of 1 cm²/ ml at 310 K for 3 days. Cells at a density of 1 \times 10⁴ cells/well were seeded in the 96-well plate with 100 μl MEM and cultured for 24 h. Then the medium was changed with the 100 μl extract for incubation of 1 day and 7 days, respectively. Cells incubated only with the MEM were as a negative control. The detailed procedures of the WST-1 experiment were the same as that described above. The absorbance was carried out using a plate reader at 450 nm

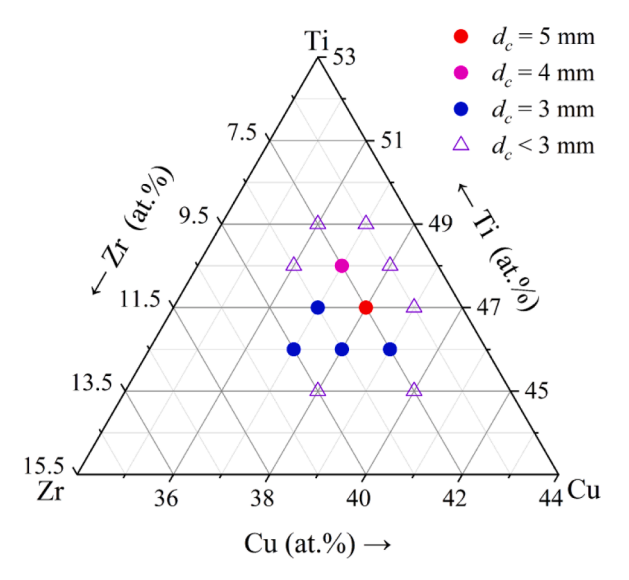
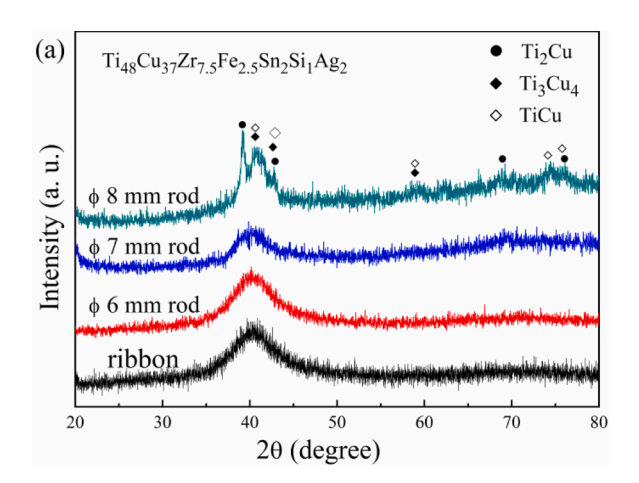


Fig. 1. Composition dependence of critical diameter (d_c) for (Ti, Cu, $Zr)_{92.5}Fe_{2.5}Sn_2Si_1Ag_2$ BMGs fabricated by injection copper-mold casting.



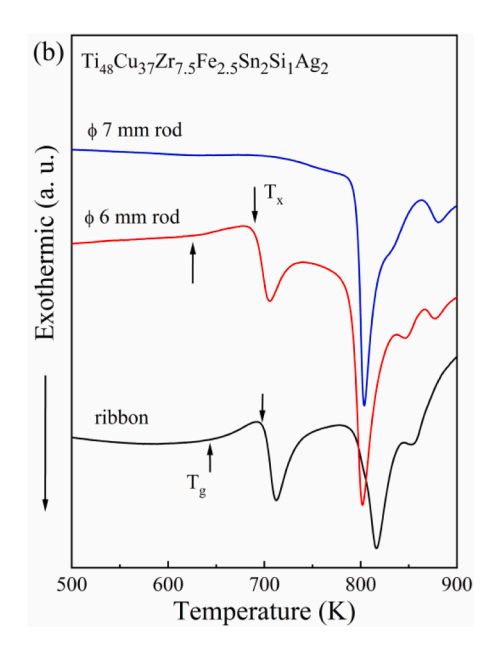
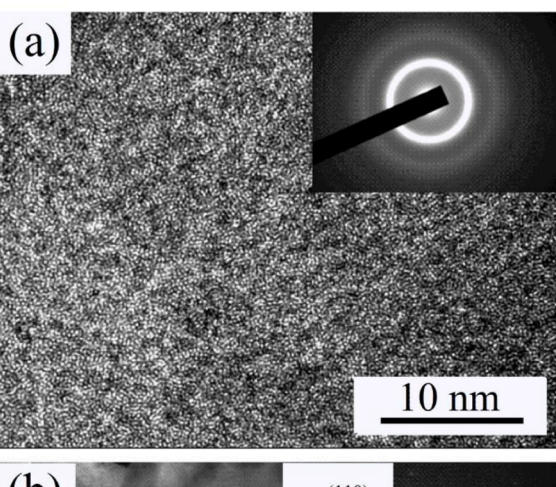


Fig. 2. (a) XRD patterns and (b) DSC curves of the ${\rm Ti_{48}Cu_{37}Zr_{7.5}MAg_2}$ cast rods and melt-spun ribbon.



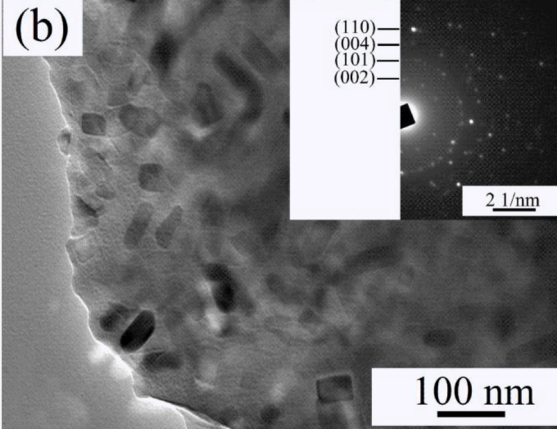


Fig. 3. TEM images with the insets showing the SAED patterns of the ${\rm Ti}_{48}{\rm Cu}_{37}{\rm Zr}_{7.5}{\rm MAg}_2$ rods with diameters of (a) 6 mm and (b) 7 mm.

(cell viability in negative control).

2.4.4. Cell differentiation and mineralization

For the osteoblast differentiation and mineralization tests, cells were cultured on quadruplicate specimens for each alloy at a density of 1×10^4 cells/well After 7-day proliferation, the cells were cultured in differentiation media composed of culture media added 8 mM β -glycer-ophosphate (MP Biomedicals), 50 µg/ml ascorbic acid, and 10^{-8} M dexamethasone (Sigma). After 21-day incubation, cell differentiation and mineralization were determined by the alkaline phosphatase (ALP) activity and calcification of the extracellular matrix (ECM), respectively.

2.4.5. Determination of ALP activity and calcification of ECM

Cell differentiation from pre-osteoblasts to osteoblasts was determined as the ALP activity. The detailed experimental procedure was the same as that presented in a previous study [33]. Briefly, cells were cultured in a lysis buffer, and then the supernatant was collected to assess the ALP activity and the total protein contents. The ALP activity was evaluated as the release of p-nitrophenol from the p-nitrophenyl phosphate. The absorbance of the specimens was recorded at 405 nm. The results of ALP activity were performed as normalization by the total protein contents obtained with a Protein Assay Reagent Kit.

Alizarin Red S staining (ARS) was used to characterize the calcification of ECM. After differentiation, the cells were washed with PBS, and then fixed with 4% paraformaldehyde for 30 min. Afterwards, the fixed cells were rinsed with PBS and stained with 2% ARS (pH 4.2). The stained specimens were rinsed with the deionized water and visualized with an optical microscope (Nikon Eclipse MA200).

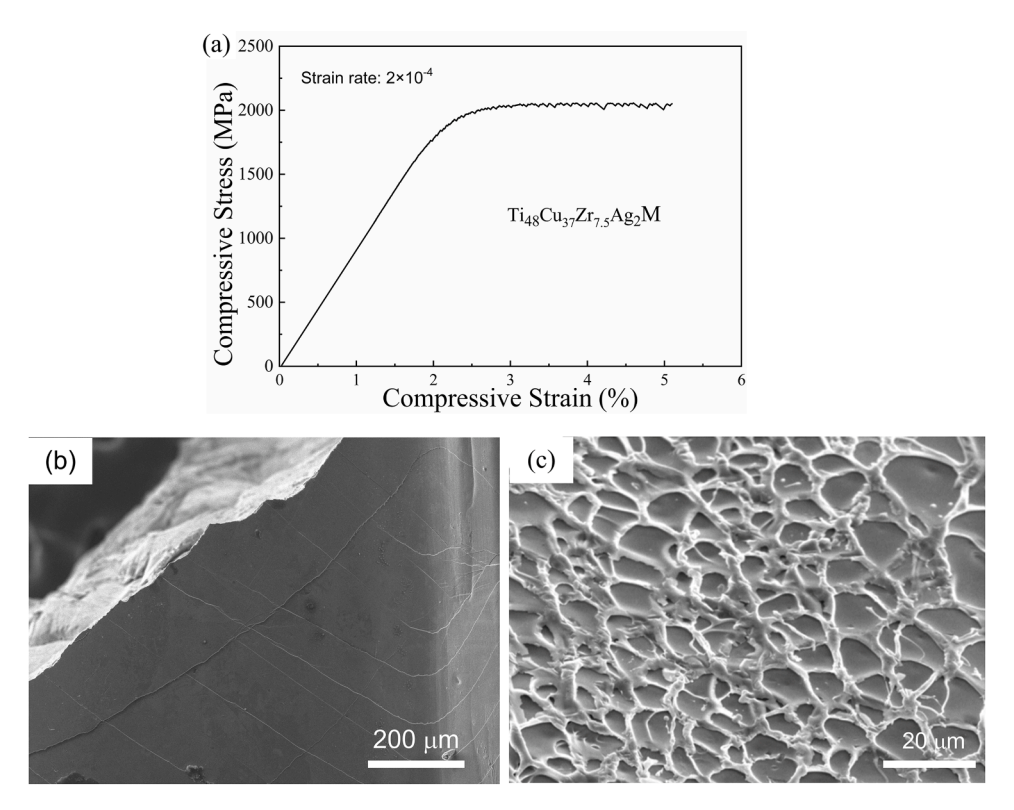


Fig. 4. (a) Engineering compressive stress–strain curve of the ${\rm Ti_{48}Cu_{37}Zr_{7.5}MAg_2}$ BMG with a diameter of 2 mm, and the SEM images of (b) the lateral and (c) the fracture surfaces of the BMG after the compressive deformation.

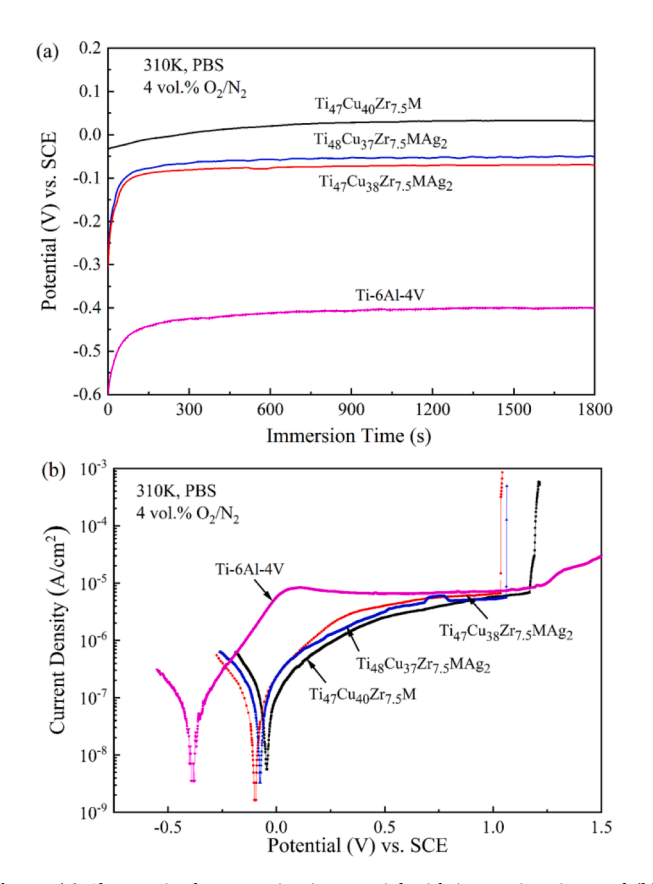


Fig. 5. (a) Changes in the open circuit potential with immersion time and (b) potentiodynamic-polarization curves of the $Ti_{47}Cu_{40}Zr_{7.5}M$ [25], $Ti_{47}Cu_{38}Zr_{7.5}MAg_2$ [29], and $Ti_{48}Cu_{37}Zr_{7.5}MAg_2$ BMGs and the Ti–6Al–4V alloy in the PBS at 310 K.

 $\label{table 1} \begin{tabular}{lll} \textbf{Values} & of & corrosion parameters derived from potentiodynamic-polarization curves & for & the & $Ti_{47}Cu_{40}Zr_{7.5}M$ & [25], & $Ti_{47}Cu_{38}Zr_{7.5}MAg_2$ & [29], & and $Ti_{48}Cu_{37}Zr_{7.5}MAg_2$ & BMGs and the Ti64 alloy in the PBS at 310 K. \end{tabular}$

Alloy	E _{corr} (V)	$i_{corr}(\times 10^{-8}$ A/cm ²)	E _{pit} (V)	E_{pit} - $E_{corr}(V)$	Corrosion rate (×10 ⁻⁴ mm/y)
Ti ₄₇ Cu ₄₀ Zr _{7.5} M	$\begin{array}{c} 0.02 \\ \pm \ 0.01 \end{array}$	$\textbf{4.7} \pm \textbf{1.4}$	1.20 ± 0.03	$\begin{array}{c} 1.18 \pm \\ 0.04 \end{array}$	4.4 ± 1.3
Ti ₄₇ Cu ₃₈ Zr _{7.5} MAg ₂	-0.11 ± 0.04	6.5 ± 0.5	0.99 ± 0.06	1.10 ± 0.08	6.5 ± 0.4
Ti ₄₈ Cu ₃₇ Zr _{7.5} MAg ₂	$\begin{array}{l} \textbf{-0.06} \\ \pm \ \textbf{0.02} \end{array}$	5.2 ± 0.9	1.04 ± 0.09	$\begin{array}{c} 1.10\ \pm\\ 0.07\end{array}$	5.1 ± 1.7
Ti64	$\begin{array}{l} \textbf{-0.44} \\ \pm \ \textbf{0.05} \end{array}$	7.5 ± 0.4	-	-	6.8 ± 0.3

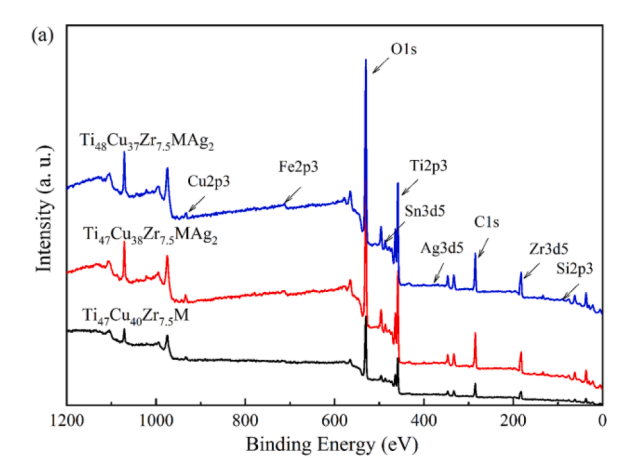
2.5. Statistical analysis

For any cellular-behavior tests, at least three samples were performed. The statistical analysis was conducted with the Student's t-test (JMP Software, USA). The differences at p < 0.05 were considered statistically significant.

3. Results

3.1. Microstructures and mechanical properties

The microstructure of the (Ti, Cu, Zr) $_{92.5}$ Fe $_{2.5}$ Sn $_{2}$ Si $_{1}$ Ag $_{2}$ rods with different diameters fabricated by injection copper-mold casting was examined by XRD. The critical diameters of the glassy alloys are shown in Fig. 1. The Ti-based metallic glasses with diameters of 3-5 mm can be formed in the composition range of 48-50 at.% Ti, 37-39 at.% Cu and



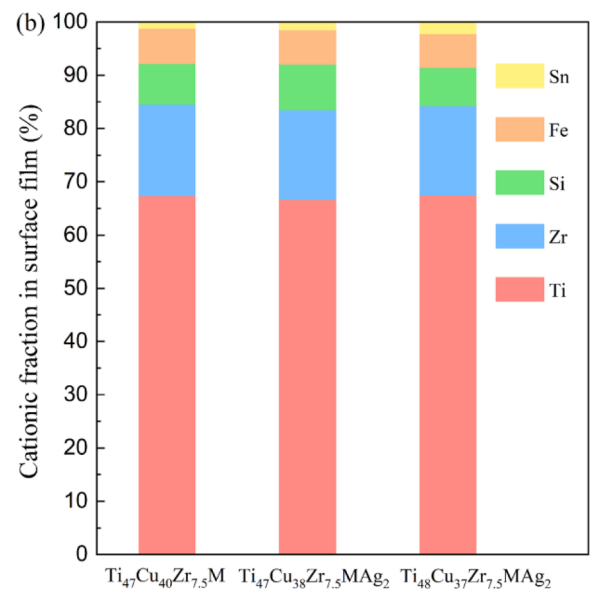


Fig. 6. (a) XPS survey spectra and (b) cationic fractions of surface films formed on the ${\rm Ti_{47}Cu_{40}Zr_{7.5}M}$, ${\rm Ti_{47}Cu_{38}Zr_{7.5}MAg_2}$, and ${\rm Ti_{48}Cu_{37}Zr_{7.5}MAg_2}$ BMGs after the 30-day immersion in the PBS at 310 K.

 $\label{eq:table 2} \begin{tabular}{ll} Table 2 \\ The concentrations (ppb) of metal ions released from the $Ti_{47}Cu_{40}Zr_{7.5}M$, $Ti_{47}Cu_{38}Zr_{7.5}MAg_2$, and $Ti_{48}Cu_{37}Zr_{7.5}MAg_2$ BMGs and the Ti64 alloy after immersion in the PBS for 30 days. \end{tabular}$

Alloy	Cu	Fe	Si	Ag	Al	V
Ti ₄₇ Cu ₄₀ Zr _{7.5} M	12	1.5	150	-	-	-
$\mathrm{Ti_{47}Cu_{38}Zr_{7.5}MAg_{2}}$	12	2.6	190	< 1	-	-
$Ti_{48}Cu_{37}Zr_{7.5}MAg_2$	19	4.5	180	< 1	-	-
Ti64	-	-	-	-	2.8	1.4

7.5 – 9.5 at.% Zr. The GFA of the Ti-based metallic glasses is sensitive to alloy compositions. It is notable the $\rm Ti_{48}Cu_{37}Zr_{7.5}MAg_2$ and $\rm Ti_{47}Cu_{38}Zr_{7.5}MAg_2$ BMGs possess high GFA with d_c up to 4 mm and 5 mm, respectively. Our previous study indicated that the $\rm Ti_{47}Cu_{38}Zr_{7.5}MAg_2$ BMG with a d_c of 7 mm can be prepared by the tilt-pouring casting method [29]. Compared with injection casting, the tilt-pouring casting with a shorter filling time and higher casting velocity is beneficial to obtaining bulk glassy samples with larger sizes [35]. In the present work, preparation of the $\rm Ti_{48}Cu_{37}Zr_{7.5}MAg_2$ rod samples with larger diameters were further performed. As given in Fig. 2(a), the XRD patterns of the $\rm Ti_{48}Cu_{37}Zr_{7.5}MAg_2$ rods with diameters of 6 mm and 7 mm present a main halo corresponding to the amorphous structure, similar

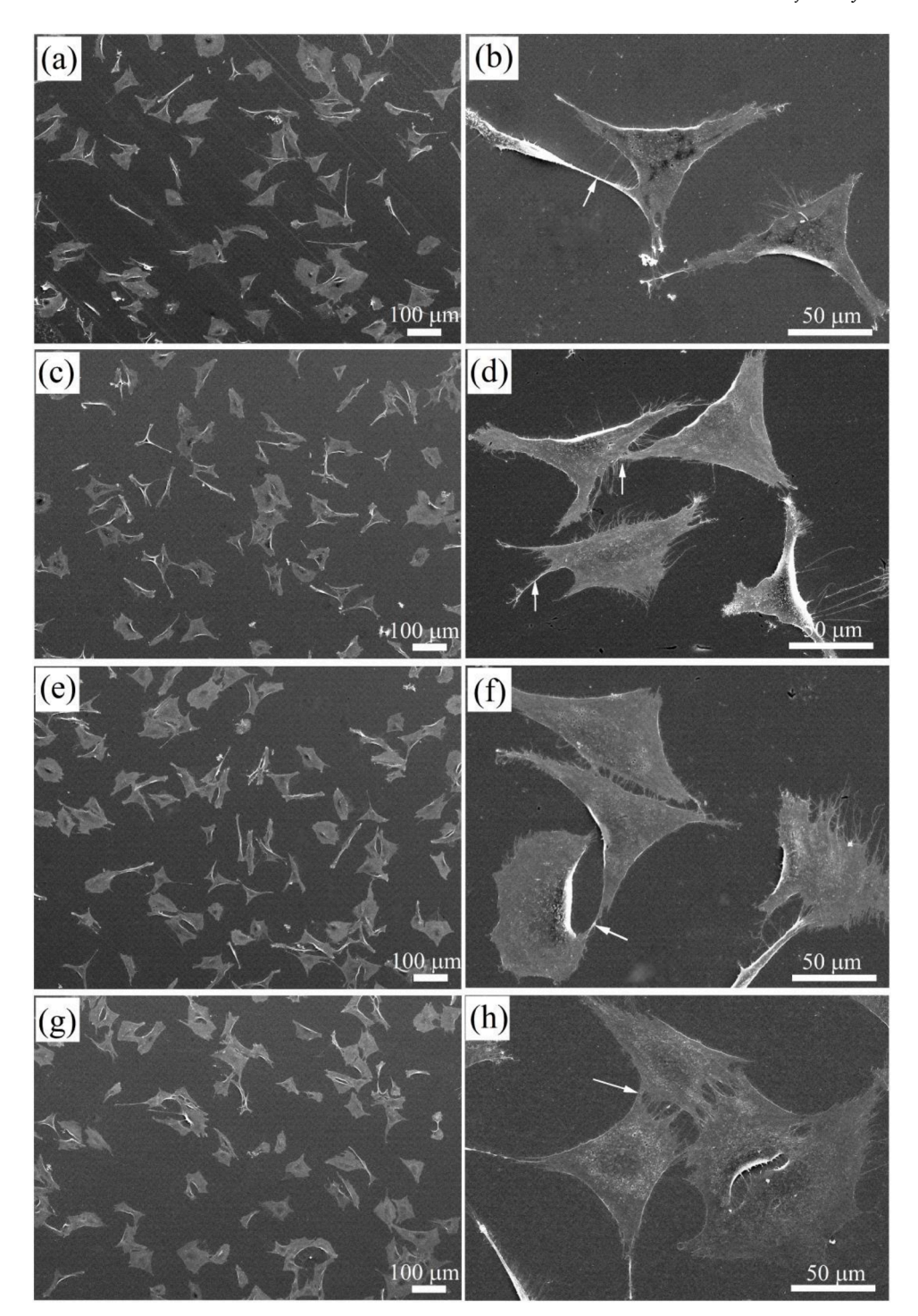
to that of a glassy ribbon sample. However, for the 8-mm-diameter rod sample, sharp crystalline peaks corresponding to Ti_2Cu , Ti_3Cu_4 , and TiCu phases are observed in the XRD pattern.

Fig. 2(b) presents the DSC plots of the alloy rods of 6 mm and 7 mm in diameter, and the DSC curve of the melt-spun ribbon is also shown for comparison, where T_g and T_X correspond to glass transition temperatures and onset temperatures of crystallization. The DSC traces of the ribbon and the 6-mm-diameter rod samples sequentially exhibit almost identical glass transition at 638 K, supercooled liquid region ($\Delta T_{\rm x} = T_{\rm x}$ - T_g) of 53 K prior to crystallization at 691 K. The large supercooled liquid region of the Ti₄₈Cu₃₇Zr_{7.5}MAg₂ BMG, similar to that of the $Ti_{47}Cu_{38}Zr_{7.5}MAg_2$ BMG ($\Delta T_x = 52$ K) [29], suggests the high thermal stability of the supercooled liquid against crystallization. However, the DSC curve of the 7-mm-diamter Ti₄₈Cu₃₇Zr_{7.5}MAg₂ rod sample exhibits the indistinctive glass transition and supercooled liquid region, indicating the precipitation of crystallites. The microstructure of the Ti₄₈Cu₃₇Zr_{7.5}MAg₂ rod samples with diameters of 6 mm and 7 mm was further examined, using TEM. As demonstrated in Fig. 3(a), the high-resolution transmission election microscopy (HRTEM) image of the 6-mm-diameter rod sample and the selected area electron diffraction (SEAD) with only halo rings demonstrate a fully-amorphous structure. The TEM bright-field image of the 7-mm-diameter rod [Fig. 3(b)] reveals that nanocrystallites with grain sizes of 10 - 30 nm are dispersed in the amorphous matrix. As presented in the inset of Fig. 3(b), the SAED pattern shows continuous spotty rings, which are identified as the tetragonal Ti₂Cu phase. Besides, the morphology of the specimen with a diameter of 6 mm after etching exhibited a uniform gray background, and no distinct contrast revealing the precipitation of a crystalline phase is seen, further confirming the amorphous structure of the 6-mm-diameter sample. Therefore, the critical diameter of the Ti₄₈Cu₃₇Zr_{7.5-} MAg₂ bulk metallic glass prepared by tilt-pouring casting is 6 mm. The novel Ti-based metallic glass with high GFA is promising as a potential biomaterial.

Fig. 4(a) displays the compression behavior of the $Ti_{48}Cu_{37}Zr_{7.5}$. MAg₂ BMG. The $Ti_{48}Cu_{37}Zr_{7.5}$ MAg₂ BMG exhibits an elastic limit of ~ 2 %, followed by yielding at about 1.94 GPa, and then deforms in a plastic manner with serrations. A plastic strain of about 2.8% prior to the fracture at 2.05 GPa is observed. The surface morphologies of the $Ti_{48}Cu_{37}Zr_{7.5}$ MAg₂ BMG after the compressive test are presented in Fig. 4(b) and (c). Many shear bands are observed of the deformed BMG. The fracture angle between the main fracture plane and the applied load is $\sim 41^{\circ}$. The fracture surface displays vein-like patterns typical of BMGs with good plasticity. The elastic modulus (*E*) of the $Ti_{48}Cu_{37}Zr_{7.5}$ MAg₂ BMG measured by the ultrasound velocity measurement were ~ 100.8 GPa. The $Ti_{48}Cu_{37}Zr_{7.5}$ MAg₂ BMG also exhibited high hardness (*Hv*) of about 571 Hv.

3.2. Bio-corrosion behavior

Fig. 5 shows the time-dependence of open-circuit potentials and the potentiodynamic-polarization plots of Ti₄₈Cu₃₇Zr_{7.5}MAg₂ BMG, together with the curves of Ti₄₇Cu₃₈Zr_{7.5}MAg₂, Ti₄₇Cu₄₀Zr_{7.5}M, and Ti64 alloys reported in Refs. [25,29]. As shown in Fig. 5(a), the OCPs of the BMGs increase abruptly initially and then achieve the constant values, implying an improved stability of the surface films during the immersion. The BMGs (around - 0.1 V) exhibit nobler OCP values than that of the Ti64 (around - 0.40 V), suggesting the higher stability of the passive films formed on the BMGs. The potentiodynamic-polarization plots of the samples are demonstrated in Fig. 5(b). Table 1 summarizes the corrosion parameters. The Ti-based BMGs are spontaneously passivated with a low passive current density (ipass) of approximately 10⁻⁶ A/cm², following a wide passive region. Pitting corrosion occurs in the potential range of $1.0\,-\,1.2\,$ V. As noticed in Table 1, the Ag-incorporated Ti-based BMGs exhibit a slightly-higher passive current density (i_{corr}), lower pitting potential (E_{pit}), corrosion potential (E_{corr}), and corrosion rates than those of the Ag-free Ti-based BMG, implying the



 $\textbf{Fig. 7.} \ \ \text{Morphologies of MC3T3-E1 cells on (a)-(b)} \ \ \text{Ti}_{47}\text{Cu}_{40}\text{Zr}_{7.5}\text{M BMG, (c)-(d)} \ \ \text{Ti}_{47}\text{Cu}_{38}\text{Zr}_{7.5}\text{MAg}_2 \ \text{BMG, (e)-(f)} \ \ \text{Ti}_{48}\text{Cu}_{37}\text{Zr}_{7.5}\text{MAg}_2 \ \text{BMG, and (g)-(h)} \ \ \text{the Ti64 alloy after incubation for 4 h.}$

negative effect of Ag microalloying on the corrosion resistance of the BMGs. Moreover, the values of the corrosion parameters of the ${\rm Ti_{48}Cu_{37}Zr_{7.5}MAg_2}$ BMG are parallel to those of the ${\rm Ti_{47}Cu_{38}Zr_{7.5}MAg_2}$ BMG, suggesting that the slightly-higher Ti/Cu ratio has little influence on the corrosion resistance. The low i_{pass} and the corrosion rates in the order of 10^{-4} mm/year indicate the good bio-corrosion resistance of the Ti-based metallic glasses.

The bio-corrosion resistance was also investigated by the immersion test. No weight loss was detected for the Ti-based BMGs, and the Ti64 after immersion in the PBS for 30 days, indicating the corrosion rates of less than 10^{-3} mm/year, which is consistent with those presented in

Table 1. For understanding the origin of the good corrosion resistance of these BMGs, the chemical composition of the oxide films formed on the surface of the $\rm Ti_{48}Cu_{37}Zr_{7.5}MAg_2$, $\rm Ti_{47}Cu_{38}Zr_{7.5}MAg_2$, $\rm Ti_{47}Cu_{40}Zr_{7.5}M$ BMGs after 30-day immersion was characterized by XPS. The peaks of C, O, Zr, Cu, Ti, Sn, Si, Fe, and Ag are found in the XPS survey spectra, as presented in Fig. 6(a). The C 1s peaks are related to the surface carbon contamination of the specimens. The cationic concentrations for the BMGs are illustrated in Fig. 6(b). In the surface films formed on the alloys, Ti, Zr, Fe, and Si are enriched, while Cu and Ag are deficient with respect to the nominal compositions after the 30-day immersion. Consequently, these results indicate that the passive films of the BMGs

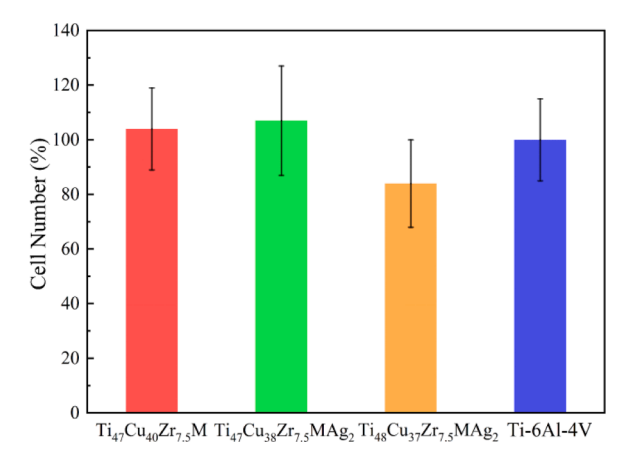


Fig. 8. Cell numbers attached to the $Ti_{47}Cu_{40}Zr_{7.5}M$, $Ti_{47}Cu_{38}Zr_{7.5}MAg_2$ and $Ti_{48}Cu_{37}Zr_{7.5}MAg_2$ BMGs and the Ti64 alloy (presented as percentages of cells attached to the Ti64 alloy) after cell culture for 4 h.

mainly consist of TiO_2 , ZrO_2 , SiO_2 and FeO/Fe_2O_3 , which is responsible for their good bio-corrosion resistance. Furthermore, the amounts of the cationic ions in the surface film of the Ag-free BMG are not significantly different from those of the Ag-incorporated BMGs, implying the similar corrosion resistance of these BMGs.

The ion concentrations of extracts of the four Ti alloys after the 30-day immersion were tested to further investigate the anti-corrosion performance and biocompatibility. As listed in Table 2, Cu, Fe, Si, and Ag ions are detected from the extracts of the Ti-based BMGs, and Al and V ions are detected from the extract of the Ti64. The BMG extracts exhibit similar concentrations of the released metallic ions. The low ion concentrations also demonstrate the good bio-corrosion resistance, which is advantageous to implant applications. Moreover, the concentrations of the released metal ions are far below the corresponding threshold values for bio-safety [36].

3.3. In vitro biocompatibility

Good biocompatibility of biomaterials is essential to avoiding harmful effects on the tissues of the human body. In this study, the *in vitro* biocompatibility of the present Ti-based BMGs was systemically evaluated. Both indirect cytotoxicity test and direct cell-culture experiments, including cell adhesion, proliferation, differentiation, and mineralization, were carried out, employing the MC3T3-E1 preosteoblasts.

3.3.1. Cell adhesion and morphology

As revealed in Fig. 7, the cells adhere on the surfaces of the $\rm Ti_{47}Cu_{40}Zr_{7.5}M$, $\rm Ti_{47}Cu_{38}Zr_{7.5}MAg_2$, and $\rm Ti_{48}Cu_{37}Zr_{7.5}MAg_2$ bulk glassy alloys and the Ti64 after the 4-hour incubation. Numerous cells are initially adhered on the different sample surfaces without regular orientation. The cells present typical polygonal and irregular shapes with the extended cytoplasm and numerous pseudopodia (as denoted by the arrows). In Fig. 8, the quantities of attached cells for all the samples are presented as the percentages of the result on the Ti64. No statistical difference is distinguished among the four Ti alloys, indicating the good cell viability on the Ti-based BMGs parallel to that on the Ti64.

The actin cytoskeleton is of great significance for controlling cell shape and supporting cell adhesion [37]. The cytoskeleton development in MC3T3-E1 pre-osteoblasts after culturing on the Ti alloys for 4 h was observed by fluorescent staining (Fig. 9). It can be found that cells adhered on the alloys exhibit similar actin cytoskeletal organizations. The actin filaments (green) are formed in various directions, mainly in the directions parallel to the cellular axises and sometimes circling the cytoplasm. The nuclei (blue) of cells on all the Ti alloys can be clearly observed without distinguishable difference. The results manifest that the Ti-based BMGs can support the normal cell adhesion and spreading of the MC3T3-E1 cells.

3.3.2. Cell proliferation and in vitro cytotoxicity evolution

The proliferation of the cells on the Ti-based alloys after the 2-, 4- and 7-day incubation are monitored, using the WST-1 assay, as

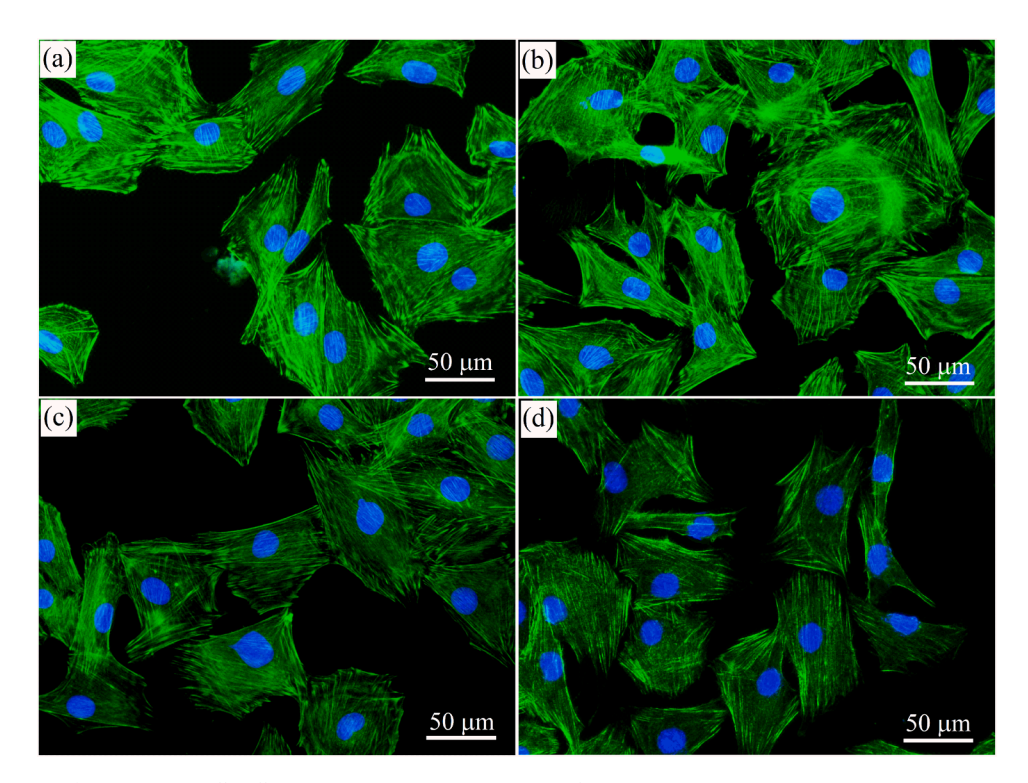


Fig. 9. Fluorescence images for MC3T3-E1 cells adherent on (a) $Ti_{47}Cu_{40}Zr_{7.5}M$ BMG, (b) $Ti_{47}Cu_{38}Zr_{7.5}MAg_2$ BMG, (c) $Ti_{48}Cu_{37}Zr_{7.5}MAg_2$ BMG, and (d) the Ti64 alloy after 4 h, showing actin filaments (green) and the nuclei (blue), respectively.

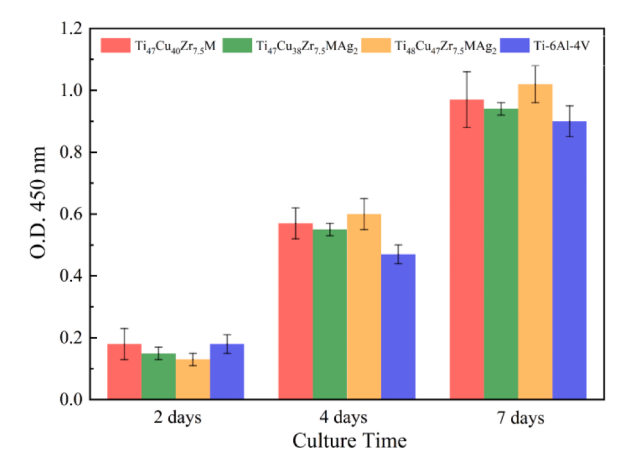


Fig. 10. Proliferation of MC3T3-E1 cells on the $Ti_{47}Cu_{40}Zr_{7.5}M$, $Ti_{47}Cu_{38}Zr_{7.5}MAg_2$, and $Ti_{48}Cu_{37}Zr_{7.5}MAg_2$ BMGs and the Ti–6Al–4V alloy after cell culture for 2, 4, and 7 days, respectively.

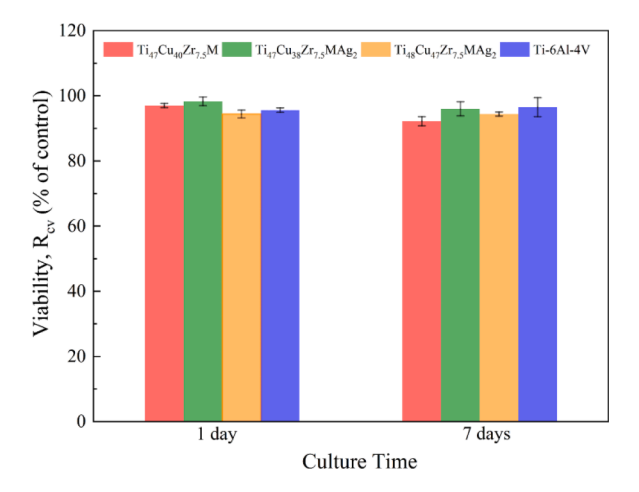


Fig. 11. Cytotoxicity of MC3T3-E1 cells cultured in the extraction media of the ${\rm Ti}_{47}{\rm Cu}_{40}{\rm Zr}_{7.5}{\rm M}$, ${\rm Ti}_{47}{\rm Cu}_{38}{\rm Zr}_{7.5}{\rm MAg}_2$, and ${\rm Ti}_{48}{\rm Cu}_{37}{\rm Zr}_{7.5}{\rm MAg}_2$ BMGs and the Ti64 alloy for 1 and 7 days.

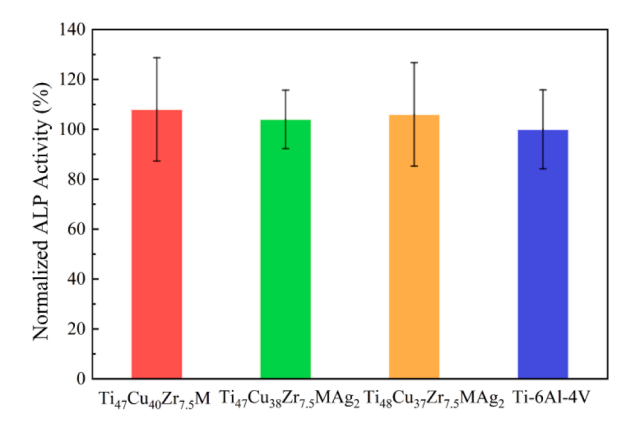


Fig. 12. Normalized ALP activities of MC3T3-E1 cell lysates after 7-day growth followed by 21-day differentiation on the alloys. Results are presented as percentages of that on the Ti64 alloy.

presented in Fig. 10. The gradually increased O.D. values from days 2 to 7, corresponding to the viable cell numbers, suggest that the cells proliferated continuously. At day 2, the O.D. value of the Ag-free BMG is slightly greater than those of the Ag-incorporated BMGs and is in

parallel to that of the Ti64. After incubation for 4 and 7 days, the cell proliferation on the Ti-based BMGs is slightly better than that on the Ti64, indicating the better cell proliferation of the BMGs. Besides, the cell proliferation test shows no statistically-significant difference for these Ti-based BMGs, indicating that the Ag microalloying and the slightly-different Ti/Cu ratios of the BMGs has no distinct influence on the cell-proliferation behavior.

The cytotoxicity of the Ti-based BMGs was evaluated by an indirect method according to ISO 10993-5:2009 [34]. The cells were cultured in the extracts for 1-7 days, and the related results presented as percentages to the results on a blank control after 1- and 7-day incubation are shown in Fig. 11. The cell viability in the extracts of the BMGs is at the same level as that in the extract of the Ti64. Additionally, the viability in all the extracts is above 90%, indicating their non-cytotoxicity.

3.3.3. Cell differentiation and mineralization

Cell differentiation is a significant performance for the MC3T3-E1 cells to reveal the osteogenic function. The ALP expression is an early sign of osteogenesis differentiation. The results of ALP activities normalized to the total protein contents are shown in Fig. 12. The cells cultured on the Ti-based BMGs present relatively-higher ALP activity than that on the Ti64, indicating that the Ti-based BMGs could support the differentiation of the cells. Additionally, the ALP activities of cells on the three Ti-based BMGs showed no statistical difference.

Fig. 13 displays the SEM images of the cells after differentiation. MC3T3-E1 cells can form thick cell multilayers with surrounding ECM on the alloys. The visual detection of mineralization of the osteoblast cells grown on the Ti alloys was characterized using ARS staining (insets in Fig. 13.) It can be qualitatively concluded that the cells can produce calcium deposits on the studied Ti alloys after 7-day incubation, followed by 21-day differentiation. Furthermore, the ARS-stained areas for the BMGs are larger than that for the Ti64, suggesting that MC3T3-E1 cells can exhibit a stronger osteogenic function on these Ti-based BMGs.

4. Discussion

The Ti-based bulk metallic glasses are promising candidates for biomedical applications, especially for orthopedic implants (e.g., artificial prostheses, bone plates, screws, and dental roots), because of their high strength, low Young's modulus, and good corrosion and wear resistance [10,21-30]. The present work indicates that (Ti, Cu, Zr)_{92.5}Fe_{2.5}Sn₂Si₁Ag₂ BMGs with diameters of 3 – 6 mm can be formed over a composition range of 48 - 50 at.% Ti, 37 - 39 at.% Cu, and 7.5 -9.5 at.% Zr, and the GFA is sensitive to the alloy compositions. The present Ti₄₈Cu₃₇Zr_{7.5}MAg₂ and the Ti₄₇Cu₃₈Zr_{7.5}MAg₂ [29] BMGs with a large d_c of 6 mm and 7 mm, respectively, can be obtained. It is well known that the large difference in the atomic size and the relatively-strong atomic attraction (relatively large negative heat of mixing) among the constituent elements may improve the GFA [38]. The (Ti, Cu, Zr)_{92.5}Fe_{2.5}Sn₂Si₁Ag₂ alloys consist of multicomponent with relatively-strong attractive interactions and large mismatch in the atomic size, including relatively-large Zr, and medium-sized Sn, Cu, Ti, Fe, and Ag, as well as small Si [39], which would improve the atomic-packing density and promote the stability of atomic clusters, leading to a high GFA [38]. Besides, the Ti₄₈Cu₃₇Zr_{7.5}MAg₂ BMG exhibits a large supercooled liquid region ($\Delta T_x = 53$ K), similar to that of the $Ti_{47}Cu_{38}Zr_{7.5}MAg_2$ BMG ($\Delta T_x = 52$ K) [29], suggesting the high stabilization of the supercooled liquid region. Additionally, the BMGs can be precisely made into applications in complex shapes by using the thermoplastic forming ability in the supercooled liquid region, which may suggest them as promising biomaterials [9,11].

The Ti-based BMGs exhibited high compressive strength up to \sim 2.05 GPa. The strength of the present Ti-based BMGs would be higher than that of the Ti64 (\sim 930 MPa) even under tension [1], since the tensile strength of metallic glasses is usually slightly lower than

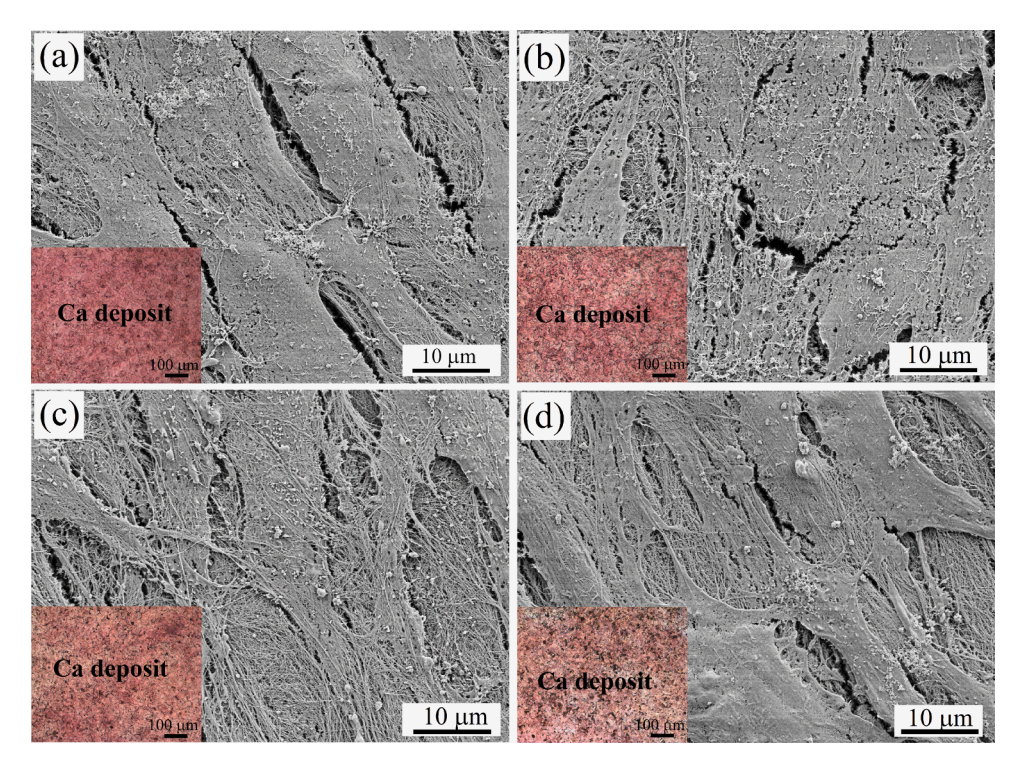


Fig. 13. SEM in-lens images of MC3T3-E1 cells cultured on (a) $Ti_{47}Cu_{40}Zr_{7.5}M$ BMG, (b) $Ti_{47}Cu_{38}Zr_{7.5}MAg_2$ BMG, (c) $Ti_{48}Cu_{37}Zr_{7.5}MAg_2$ BMG, and (d) the Ti64 alloy after 7-day growth, followed by 21-day differentiation (insets: ARS Ca-staining visualized ECM).

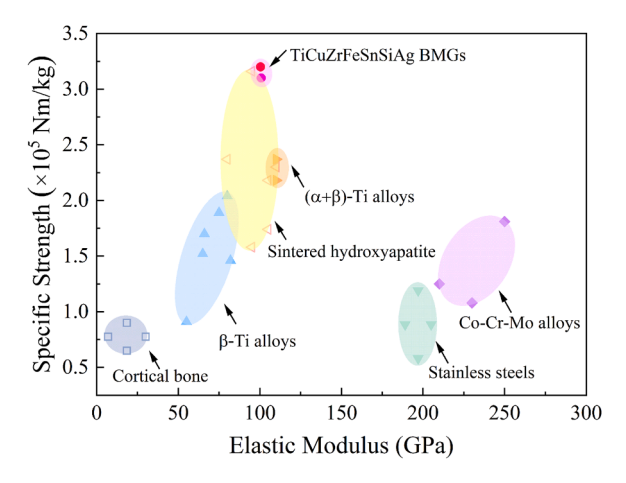


Fig. 14. Comparison of mechanical properties among the Ti-based BMGs and some typical biomedical materials [2,3,5,29,41].

compressive fracture strength [40]. High specific strength is also required for load-bearing biomaterials, especially those served as joint or dental implants, which can reduce the implant dimensions and mitigate immune rejection and host tissue damage. Fig. 14 illustrates the specific strength and the elastic moduli of the Ti-Zr-Cu-Fe-Sn-Si-Ag BMGs and some typical biomaterials as well as cortical bone [2,3,5,29, 41]. The specific strengths of these Ti-based bulk glassy alloys are higher than those of the crystalline titanium alloys, Co-Cr-Mo alloys, and stainless steels. In addition, high fatigue strength of the Ti-based BMGs can be expected [42,43], which would be favorable for the biomedical applications. Furthermore, these Ti-based bulk glassy alloys possess lower elastic moduli of ~ 100 GPa in comparison with that of the Ti64 110 GPa) [3], which is advantageous for mitigating the stress-shielding effect of the implants. The β-Ti alloys possess lower elastic moduli, whereas the strength and hardness reduce concurrently [44]. In comparison, the Ti-based BMGs presented high hardness in the

range of 571-590~Hv. Their high ratio of hardness to elastic modulus (H/E) may also lead to good wear resistance of the Ti-based BMGs in the simulated physiological environment, which may alleviate the risk of particle disease during the implantation [30]. The high strength, low elastic moduli, and good wear performance would make the present Ti-based metallic glasses suitable for biomedical applications from the perspective of mechano-compatibility.

Good corrosion resistance is also an essential feature of metallic biomaterials to inhibit the release of metallic ions into the tissue and maintain the implant integrity during service in the aggressive physiological environment. The results of the immersion and electrochemical measurements in the PBS demonstrated the great anti-corrosion performance of the Ti-based bulk glassy alloys, i.e., higher E_{corr} , and lower i_{corr} and i_{pass} than those of the Ti64. For the Ti-based BMGs, although occurrence of pitting corrosion is recognized at high potentials above 1.0 V (vs. SCE) during anodic polarization, their corrosion rates are similar to that of the Ti64, suggesting their similar capability of withstanding in the aggressive physiological fluid. On the basis of the abovementioned XPS results (Fig. 6), the surface films of the BMGs after 30-day immersion in the PBS are mainly consisted of TiO₂, ZrO₂, SiO₂, and FeO/Fe₂O₃. The TiO₂, ZrO₂, and SiO₂ are chemically stable, which are responsible for the great corrosion resistance of these Ti-based BMGs [25,35,45]. It has also been reported that the TiO₂ oxide adopted with Si would reduce the diffusion coefficient of oxygen and resulted in a higher resistance to oxygen penetration in the passive film based on the point-defect model [45,46]. Meanwhile, the unique amorphous feature of the BMGs may provide the formation of uniform passive films [47]. As mentioned above, the Ti-based BMGs suffered pitting corrosion at high potentials, which is attributed to the susceptibility of ZrO2 to the chloride containing solutions [48]. Whereas the passive films are sufficiently protective to hinder the release of metallic ions into the PBS, which can be revealed by the ICP-MS results (Table 2) and negligible weight loss after the long-term immersion. Thus, the great bio-corrosion resistance of the Ti-Cu-Zr-Fe-Sn-Si(-Ag) BMGs, is considered sufficient for biomedical implants.

In vitro cellular responses to the present Ti-based BMGs were

employed to study their biocompatibility. As revealed by the results of the cell-culture tests, the BMGs can support the cell adhesion and proliferation, suggesting the initial biosafety of the present glassy alloys [33,49-51]. The Ti-based BMGs can also support the regular functions of MC3T3-E1 pre-osteoblasts, such as cell differentiation and mineralization. Additionally, no significant difference is found in the cell responses to these Ti-based BMGs with different compositions, implying the indistinctive influence of the minor Ag addition and the slight difference in Ti/Cu ratios on the biocompatibility. The indirect cell-culture study revealed that similar to the Ti64, the Ti-based BMGs exhibited cytotoxicity of Grade 0-1 (according to ISO 10993-5:2009 [34]), suggesting their biosafety for the application as biomaterials. The good biocompatibility of these BMGs can be mainly due to the formation of the protective passive surface films mainly composed of the biocompatible elements [15,35,50,51]. Furthermore, the high corrosion resistance would also guarantee the good biocompatibility by effectively maintaining the mechanical integrality for a long life during implantation [12.15.25.52.53].

Additionally, the present (Ti, Cu, Zr)_{92.5}Fe_{2.5}Sn₂Si₁Ag₂ BMGs are free from highly-toxic elements Be and Ni, which is blamed for the occurrence of an allergy and has antiproliferative effects on cell cultures. There are a lot of controversies about element Cu used in biomedical applications. On one hand, it has been reported that the excessive Cu might affect the cell growth and proliferation [54,55]. On the other hand, some Cu-containing stainless steels and Ti-Cu alloys can exhibit good mechanical properties and antibacterial activity induced by Cu alloying [56-58]. Furthermore, in vitro cytotoxicity studies and animal implantation have demonstrated the good biocompatibility and antibacterial effects of Cu-containing BMGs [12,13,25,59]. Meanwhile, silver and its ions possess well-established anti-bacterial properties with a broad spectrum of antimicrobial activities [60-62]. The combination of the low Ag content and great bio-corrosion resistance would lead to their bacteria-killing behavior and minimize the potential cytotoxicity concurrently. Thus, the current Ti-based BMGs with the good biocompatibility and the potential anti-bacterial property are promising biomedical materials.

5. Conclusions

In the present study, the Ti-based BMGs with diameters of 3-6 mm have been synthesized in the Ni-free (Ti, Cu, Zr)92.5Fe2.5Sn2Si1Ag2 alloy system over a wide composition range by copper-mold casting. Especially, the Ti48Cu37Zr7.5Fe2.5Sn2Si1Ag2 BMG can be prepared into the BMG rod with a diameter up to 6 mm. The novel Ti-based BMG shows a high strength (~ 2.05 GPa), high specific strength ($\sim 3.1 \times 10^5$ N m/kg), low elastic modulus (~ 100 GPa), and high microhardness (~ 571 Hv). The great bio-corrosion resistance of Ti-based BMGs revealed by low corrosion rates and corrosion densities are attributed to the formation of passive films consisted of the Ti-, Zr-, Si-, and Fe-oxides. The results of the indirect cytotoxicity test and direct cell-culture experiments demonstrate the good biocompatibility of the Ti-based metallic glasses. All these findings indicate that the Ti–Cu–Zr–Fe–Sn–Si–Ag BMGs are promising candidates for biomaterials.

Declaration of Competing Interest

The authors declare the following financial interests/personal relationships which may be considered as potential competing interests

Acknowledgements

The present work was financially supported by the National Natural Science Foundation of China (Grant No. 51671008) and the 111 Project (B17002). P. K. L. very much appreciates the supports from the National Science Foundation [DMR-1611180 and 1809640] with the program directors, Drs. Judith Yang, Gary Shiflet, and Diana Farkas.

References

- [1] Q. Chen, G.A. Thouas, Metallic implant biomaterials, Mater. Sci. and Eng. R Rep. 87 (2015) 1–57.
- [2] M. Niinomi, Recent metallic materials for biomedical applications, Metall. Mater. Trans. A 33 (2002) 477–486.
- [3] M. Long, H.J. Rack, Titanium alloys in total joint replacement—a materials science perspective. Biomaterials 19 (1998) 1621–1639.
- [4] J.S. Temenoff, A.G. Mikos, Biomaterials: The Intersection of Biology and Materials Science, Pearson/Prentice Hall, 2008.
- [5] M. Geetha, A.K. Singh, R. Asokamani, A.K. Gogia, Ti based biomaterials, the ultimate choice for orthopaedic implants – A review, Prog. Mater. Sci. 54 (2009) 397–425
- [6] T. Hanawa, Research and development of metals for medical devices based on clinical needs, Sci. Technol. Adv. Mater. 13 (2012), 064102.
- [7] J.W. Park, H.K. Kim, Y.J. Kim, J.H. Jang, H. Song, T. Hanawa, Osteoblast response and osseointegration of a Ti–6Al–4V alloy implant incorporating strontium, Acta Biomater, 6 (2010) 2843–2851.
- [8] M. Abdel-Hady Gepreel, M. Niinomi, Biocompatibility of Ti-alloys for long-term implantation, J. Mech. Behav. Biomed. Mater. 20 (2013) 407–415.
- [9] J. Schroers, Processing of bulk metallic glass, Adv. Mater. 22 (2010) 1566–1597.
- [10] H.F. Li, Y.F. Zheng, Recent advances in bulk metallic glasses for biomedical applications. Acta Biomater. 36 (2016) 1–20.
- [11] G. Kumar, H.X. Tang, J. Schroers, Nanomoulding with amorphous metals, Nature 457 (2009) 868–872.
- [12] Y.B. Wang, H.F. Li, Y. Cheng, Y.F. Zheng, L.Q. Ruan, In vitro and in vivo studies on Ti-based bulk metallic glass as potential dental implant material, Mater. Sci. Eng. C 33 (2013) 3489–3497.
- [13] H.F. Li, Y.B. Wang, Y.F. Zheng, J.P. Lin, Osteoblast response on Ti- and Zr-based bulk metallic glass surfaces after sand blasting modification, J. Biomed. Mater. Res. Part B 100 (2012) 1721–1728.
- [14] B. Zberg, P.J. Uggowitzer, J.F. Löffler, MgZnCa glasses without clinically observable hydrogen evolution for biodegradable implants, Nat. Mater. 8 (2009) 887–891.
- [15] Y. Liu, Y. Wang, H. Pang, Q. Zhao, L. Liu, A Ni-free ZrCuFeAlAg bulk metallic glass with potential for biomedical applications, Acta Biomater. 9 (2013) 7043–7053.
- [16] J.M. Park, H.J. Chang, K.H. Han, W.T. Kim, D.H. Kim, Enhancement of plasticity in Ti-rich Ti-Zr-Be-Cu-Ni bulk metallic glasses, Scr. Mater. 53 (2005) 1-6.
- [17] S.F. Zhao, N. Chen, P. Gong, K.F. Yao, New centimeter-sized quaternary Ti–Zr–Be–Cu bulk metallic glasses with large glass forming ability, J. Alloys Compd. 647 (2015) 533–538.
- [18] Y.C. Kim, W.T. Kim, D.H. Kim, A development of Ti-based bulk metallic glass, Mater. Sci. Eng. A (2004) 127–135, 375-377.
- [19] J.L. Gu, X.L. Yang, A.L. Zhang, Y. Shao, S.F. Zhao, K.F. Yao, Centimeter-sized Tirich bulk metallic glasses with superior specific strength and corrosion resistance, J. Non-Cryst. Solids 512 (2019) 206–210.
- [20] S.F. Lin, D.M. Liu, Z.W. Zhu, D. Li, H.M. Fu, Y.X. Zhuang, H.W. Zhang, H. Li, A. M. Wang, H.F. Zhang, New Ti-based bulk metallic glasses with exceptional glass forming ability, J. Non-Cryst. Solids. 502 (2018) 71–75.
- [21] Y. Guo, I. Bataev, K. Georgarakis, A.M. Jorge, R.P. Nogueira, M. Pons, A.R. Yavari, Ni- and Cu-free Ti-based metallic glasses with potential biomedical application, Intermetallics 63 (2015) 86–96.
- [22] M. Calin, A. Gebert, A.C. Ghinea, P.F. Gostin, S. Abdi, C. Mickel, J. Eckert, Designing biocompatible Ti-based metallic glasses for implant applications, Mater. Sci. Eng. C 33 (2013) 875–883.
- [23] J.J. Lai, Y.S. Lin, C.H. Chang, T.Y. Wei, J.C. Huang, Z.X. Liao, C.H. Lin, C.H. Chen, Promising Ta-Ti-Zr-Si metallic glass coating without cytotoxic elements for bioimplant applications, Appl. Surf. Sci. 427 (2018) 485–495.
- [24] G. Wang, H.B. Fan, Y.J. Huang, J. Shen, Z.H. Chen, A new TiCuHfSi bulk metallic glass with potential for biomedical applications, Mater. Des. 54 (2014) 251–255.
- [25] Y. Liu, S.J. Pang, H.F. Li, Q. Hu, B. Chen, T. Zhang, Formation and properties of Ti-based Ti-Zr-Cu-Fe-Sn-Si bulk metallic glasses with different (Ti+Zr)/Cu ratios for biomedical application, Intermetallics 72 (2016) 36–43.
- [26] M. Calin, J. Vishnu, P. Thirathipviwat, M.M. Popa, M. Krautz, G. Manivasagam, A. Gebert, Tailoring biocompatible Ti-Zr-Nb-Hf-Si metallic glasses based on highentropy alloys design approach, Mater. Sci. Eng. C 121 (2021), 111733.
- [27] T.H. Li, P.C. Wong, S.F. Chang, P.H. Tsai, J.S.C. Jang, J.C. Huang, Biocompatibility study on Ni-free Ti-based and Zr-based bulk metallic glasses, Mater. Sci. Eng. C 75 (2017) 1–6.
- [28] S.L. Zhu, X.M. Wang, F.X. Qin, A. Inoue, A new Ti-based bulk glassy alloy with potential for biomedical application, Mater. Sci. Eng. A 459 (2007) 233–237.
- [29] S.J. Pang, Y. Liu, H.F. Li, L.L. Sun, Y. Li, T. Zhang, New Ti-based Ti-Cu-Zr-Fe-Sn-Si-Ag bulk metallic glass for biomedical applications, J. Alloys Compd. 625 (2015) 323–327.
- [30] Y. Liu, S.J. Pang, W. Yang, N.B. Hua, P.K. Liaw, T. Zhang, Tribological behaviors of a Ni-free Ti-based bulk metallic glass in air and a simulated physiological environment, J. Alloys Compd. 766 (2018) 1030–1036.
- [31] S. Hiromoto, A.P. Tsai, M. Sumita, T. Hanawa, Effects of surface finishing and dissolved oxygen on the polarization behavior of Zr₆₅Al_{7.5}Ni₁₀Cu_{17.5} amorphous alloy in phosphate buffered solution, Corros. Sci. 42 (2000) 2167–2185.
- [32] ASTM-G31-72: standard practice for laboratory immersion corrosion testing of metals, Annual Book of ASTM Standards, American Society for Testing and Materials, Philadelphia, PA, USA, 2017.
- [33] L. Huang, Z. Cao, H.M. Meyer, P.K. Liaw, E. Garlea, J.R. Dunlap, T. Zhang, W. He, Responses of bone-forming cells on pre-immersed Zr-based bulk metallic glasses: Effects of composition and roughness, Acta Biomater 7 (2011) 395–405.

- [34] ISO 10993-5:2009 Biological Evaluation of Medical Devices-Part 5: Tests for In Vitro Cytotoxicity, International Organization for Standardization, Geneva, Switzerland. 2009.
- [35] Y. Liu, G. Wang, H. Li, S.J. Pang, K.W. Chen, T. Zhang, Ti-Cu-Zr-Fe-Sn-Si-Sc bulk metallic glasses with good mechanical properties for biomedical applications, J. Alloys Compd. 679 (2016) 341–349.
- [36] A. Yamamoto, R. Honma, M. Sumita, Cytotoxicity evaluation of 43 metal salts using murine fibroblasts and osteoblastic cells, J. Biomed. Mater. Res. Part A 39 (1998) 331–340.
- [37] D.A. Fletcher, R.D. Mullins, Cell mechanics and the cytoskeleton, Nature 463 (2010) 485–492.
- [38] A. Inoue, Stabilization of metallic supercooled liquid and bulk amorphous alloys, Acta Mater 48 (2000) 279–306.
- [39] A. Takeuchi, A. Inoue, Classification of bulk metallic glasses by atomic size difference, heat of mixing and period of constituent elements and its application to characterization of the main alloying element, Mater. Trans. JIM 46 (2005) 2817–2829.
- [40] Z.F. Zhang, J. Eckert, L. Schultz, Difference in compressive and tensile fracture mechanisms of Zr₅₉Cu₂₀Al₁₀Ni₈Ti₃ bulk metallic glass, Acta Mater 51 (2003) 1167–1179
- [41] E. El-Meliegy, R. Van Noort, Glasses and Glass Ceramics for Medical Applications, Springer, New York, USA, 2012.
- [42] X.D. Wang, S.L. Song, Z.W. Zhu, H.F. Zhang, X.C. Ren, Fatigue behavior of a Ti-based metallic glass: effect of sampling location in association with free volume, J. Alloys Compd. 861 (2021), 158432.
- [43] X.D. Wang, P. Liu, Z.W. Zhu, H.F. Zhang, X.C. Ren, High fatigue endurance limit of a Ti-based metallic glass, Intermetallics 119 (2020), 106716.
- [44] G. He, J. Eckert, Q.L. Dai, M.L. Sui, W. Löser, M. Hagiwara, E. Ma, Nanostructured Ti-based multi-component alloys with potential for biomedical applications, Biomaterials 24 (2003) 5115–5120.
- [45] Z. Jiang, X. Dai, H. Middleton, Effect of silicon on corrosion resistance of Ti–Si alloys, Mater. Sci. Eng. B 176 (2011) 79–86.
- [46] D.D. Macdonald, S.R. Biaggio, H. Song, Steady-state passive films: interfacial kinetic effects and diagnostic criteria, J. Electrochem. Soc. 139 (1992) 170–177.
- [47] K. Hashimoto, P. Park, J. Kim, H. Yoshioka, H. Mitsui, E. Akiyama, H. Habazaki, A. Kawashima, K. Asami, Z. Grzesik, S. Mrowec, Recent progress in corrosionresistant metastable alloys, Mater. Sci. Eng. A 198 (1995) 1–10.
- [48] Y. Liu, H.J. Wang, S.J. Pang, T. Zhang, Ti–Zr–Cu–Fe–Sn–Si–Ag–Ta bulk metallic glasses with good corrosion resistance as potential biomaterials, Rare Met., 39 (2020) 688–694.

- [49] S.K. Kolawole, W. Hai, S. Zhang, Z. Sun, M.A. Siddiqui, I. Ullah, W. Song, F. Witte, K. Yang, Preliminary study of microstructure, mechanical properties and corrosion resistance of antibacterial Ti-15Zr-xCu alloy for dental application, J. Mater. Sci. Technol. 50 (2020) 31-43.
- [50] H.H. Huang, Y. Sun, C. Wu, C. Liu, P.K. Liaw, W. Kai, Corrosion resistance and biocompatibility of Ni-free Zr-based bulk metallic glass for biomedical applications, Intermetallics 30 (2012) 139–143.
- [51] N.B. Hua, L. Huang, W. Chen, W. He, T. Zhang, Biocompatible Ni-free Zr-based bulk metallic glasses with high-Zr-content: Compositional optimization for potential biomedical applications, Mater. Sci. Eng. C 44 (2014) 400–410.
- [52] Y.S. Sun, W. Zhang, W. Kai, P.K. Liaw, H.H. Huang, Evaluation of Ni-free Zr-Cu-Fe-Al bulk metallic glass for biomedical implant applications, J. Alloys Compd. 586 (2014) S539-S543.
- [53] N.B. Hua, X.S. Hong, L.Y. Lin, Z.L Liao, L. Zhang, X.Y. Ye, Q.T. Wang, Mechanical, corrosion, and wear performances of a biocompatible Ti-based glassy alloy, J. Non-Cryst. Solids 543 (2020), 120116.
- [54] L.C. Carvalho do Lago, A.C. Matias, C.S. Nomura, G. Cerchiaro, Radical production by hydrogen peroxide/bicarbonate and copper uptake in mammalian cells: Modulation by Cu(II) complexes, J. Inorg. Biochem. 105 (2011) 189–194.
- [55] J.Y. Uriu-Adams, C.L. Keen, Copper, oxidative stress, and human health, Mol. Aspects. Med. 26 (2005) 268–298.
- [56] I.T. Hong, C.H. Koo, Antibacterial properties, corrosion resistance and mechanical properties of Cu-modified SUS 304 stainless steel, Mater. Sci. Eng. A 393 (2005) 213–222.
- [57] E. Zhang, L. Zheng, J. Liu, B. Bai, C. Liu, Influence of Cu content on the cell biocompatibility of Ti–Cu sintered alloys, Mater. Sci. Eng. C 46 (2015) 148–157.
- [58] S.Moniri Javadhesaria, S. Alipourb, M.R. Akbarpourc, Biocompatibility, osseointegration, antibacterial and mechanical properties of nanocrystalline Ti-Cu alloy as a new orthopedic material, Coll. Surf. B Biointerfaces 189 (2020), 110889.
- [59] L. Huang, E.M. Fozo, T. Zhang, P.K. Liaw, W. He, Antimicrobial behavior of Cubearing Zr-based bulk metallic glasses, Mater. Sci. Eng. C 39 (2014) 325–329.
- [60] S. Naseri, W.C. Lepry, V.B. Maisuria, N. Tufenkji, S.N. Nazhat, Development and characterization of silver-doped sol-gel-derived borate glasses with anti-bacterial activity, J. Non. Cryst. Solids. 505 (2019) 438–446.
- [61] A. Shivaram, S. Bose, A. Bandyopadhyay, Understanding long-term silver release from surface modified porous titanium implants, Acta Biomater. 58 (2017) 550–560.
- [62] R. Kumar, H. Münstedt, Silver ion release from antimicrobial polyamide/silver composites, Biomaterials 26 (2005) 2081–2088.